Cross-link of telechelic diacrylate polyethylene-glycol in peptide-based Fmoc-FF hydrogel matrices

Article

Accepted Version

Rosa, E., Pellegrino, P. ORCID: https://orcid.org/0000-0001-6018-3548, Cascione, M., Rinaldi, R. ORCID: https://orcid.org/0000-0003-2798-9341, Gianolio, E. ORCID: https://orcid.org/0000-0002-7130-4445, Edwards-Gayle, C. ORCID: https://orcid.org/0000-0001-7757-107X, Hamley, I. W. ORCID: https://orcid.org/0000-0002-4549-0926, Morelli, G., Accardo, A. and Diaferia, C. (2024) Cross-link of telechelic diacrylate polyethylene-glycol in peptide-based Fmoc-FF hydrogel matrices. ACS Applied Polymer Materials, 6 (12). pp. 7197-7208. ISSN 2637-6105 doi: 10.1021/acsapm.4c01059 Available at https://centaur.reading.ac.uk/116834/

Cross-link of diacrylate α-/ω-substituted polyethylene-glycol in Fmoc-FF hydrogel matrices.

Elisabetta Rosa,[1] Paolo Pellegrino,[2,3] Mariafrancesca Cascione[3,4] Rosaria Rinaldi[3,4] Eliana Gianolio,[5] Charlotte Edwards-Gayle,[6] Ian Hamley,[6] Giancarlo Morelli,[1] Antonella Accardo,[1,*] Carlo Diaferia[1,*]

[1]*Department of Pharmacy, Research Centre on Bioactive Peptides (CIRPeB), University of Naples "Federico II", Via T. De Amicis 95, 80145 Naples, Italy.*

[2]*Istituti Clinici Scientifici Maugeri IRCCS of Telese Terme Institute, 82037 Telese Terme, Italy.*

[3]*Institute for Microelectronics and Microsystems (IMM), CNR, Via Monteroni, 73100 Lecce, Italy.*

[4]*Department of Mathematics and Physics "Ennio De Giorgi", University of Salento, Via Monteroni, 73100 Lecce, Italy.*

[5]*Department of Molecular Biotechnology and Health Sciences, University of Turin, Turin 10126, Italy.*

[6]*School of Chemistry, Pharmacy and Food Biosciences, University of Reading, Berkshire RG6 6AD, United Kingdom.*

Reference to: antonella.accardo@unina.it *and* carlo.diaferia@unina.it

Keywords: Fmoc-FF, hydrogels, peptide materials, interpenetrating network, PEGDA

Abstract

Novel hydrogels (HGs) with enhanced structural and mechanical properties can be generated by combining two or more different building blocks in the same matrix. It has been widely demonstrated that the addition of peptides, proteins, sugars, or polymers to the low molecular weight hydrogelator Fmoc-FF [(fluorenyl methyloxycarbonyl)-diphenilalanine] can significantly modify the chemical and structural features of resulting HGs. In this context, it has been previously described the formulation of multicomponent HGs, in which Fmoc-FF is mixed to diacrylate α-/ω-substituted polyethylene-glycol derivatives (PEGDAs) with a molecular weight of 575 (PEGDA1) or 250 Da (PEGDA2). Here, we investigate the possibility to generate Fmoc-FF based interpenetrated networks performing the crosslink reaction of PEGDAs monomer in supramolecular peptide hydrogels. This approach can allow the modulation of the final properties of the material, in terms of water behaviour, topography and rigidity. Results indicate that the polymerization time, the polymer length, and the Fmoc-FF/PEGDA ratio play a crucial role into the chemistry of the materials, and, consequently, of their potential application.

Introduction

Peptides and proteins are examples of molecular entities able to generate a variety of supramolecular systems and biomaterials, coupled to biological functions.[1-6] The molecular driving forces governing their formation are predominantly non-covalent interactions, involving specific mutual recognition of molecular building blocks.[7,8] Applying a biomimicry approach, the self-assembly of synthetic peptides allows artificially replicating the aggregation pathway in nature, developing novel functional nanostructured materials, differing in shapes and morphologies.[9-13] Peptide aggregation may also lead to macroscopical hydrogels (HGs) bulk materials, self-supporting biphasic matrices with a no-Newtonian flow behavior.[14-16] Different chemical classes of peptides have been proposed as low molecular weight (LMW) gelators, and N^{α}-Fmoc (fluorenyl methyloxycarbonyl) capped peptides are some of them.[17,18] Strictly related to diphenylalanine (FF) homodimer, Fmoc-FF (**Figure 1A**) is a suitable building block for the formulation of hydrogelated matrices useful for different applicative aims. Fmoc-FF hierarchically self-organizes into β-sheet secondary structures, generating an antiparallel π-stacking of the fluorenyl groups. Because of a lateral interlocking of four twisted antiparallel β-strands, elongated nanocylindrics (external diameter of ∼3.0 nm) are formed.[19] Further lateral self-associations of these structures, forming large flat ribbons, allow the formation of the three-dimensional hydrogel matrix, formed by an entrapping water network. The interest towards Fmoc-FF peptide as basic constituent of hydrogels is related to its advantages, which include the capability to gel under very different conditions, the easy and well-assessed preparation procedure, the possibility to achieve hydrogels with a high reproducibility, and the fast gelation kinetics.[20,21] Gelation of this peptide can be induced by the change/modification of the initial chemical/physical conditions, in terms of pH (pH-switch method), chemical structure (enzymatic switch) or solvents (solvent-switch).[20] The solvent-switch methodology involves the initial Fmoc-FF dissolution at high concentration (100 mg/mL) into an organic solvent (DMSO, ethanol or HFIP), followed by the addition of water, triggering the gel formation.[22-25] Solvent-switch from organic phase to aqueous one permits the inclusion of both hydrophilic and hydrophobic elements, producing multicomponent matrices. The interest about Fmoc-FF is confirmed by the design of other chemically related analogues, too.[26] Simultaneously, the research also moved towards the development of multicomponent systems in which the Fmoc-FF peptide is mixed with other peptide sequences, organic molecules, sugars, and proteins.[27] In this context, we previously described the behaviour of Fmoc-FF HGs incorporating diacrylate α-/ω-substituted polyethylene-glycol polymers (PEGDAs, **Figure 1A**).[28] Specifically, these matrices contain alternatively two PEGDAs, namely PEGDA1 and PEGDA2 (mean molecular weight of 575 and 250 Da, respectively), and are prepared at different peptide/polymer molar ratios (1/1, 1/2, 1/5, 1/10 *mol/mol*). It is worth mentioning that the two selected

PEGDA have a MW< 1000 g/mol, needed to avoid the formation of the crystalline phases.[29] The resulting self-supporting hydrogels exhibited a mechanical response in the 2-8 kPa range.

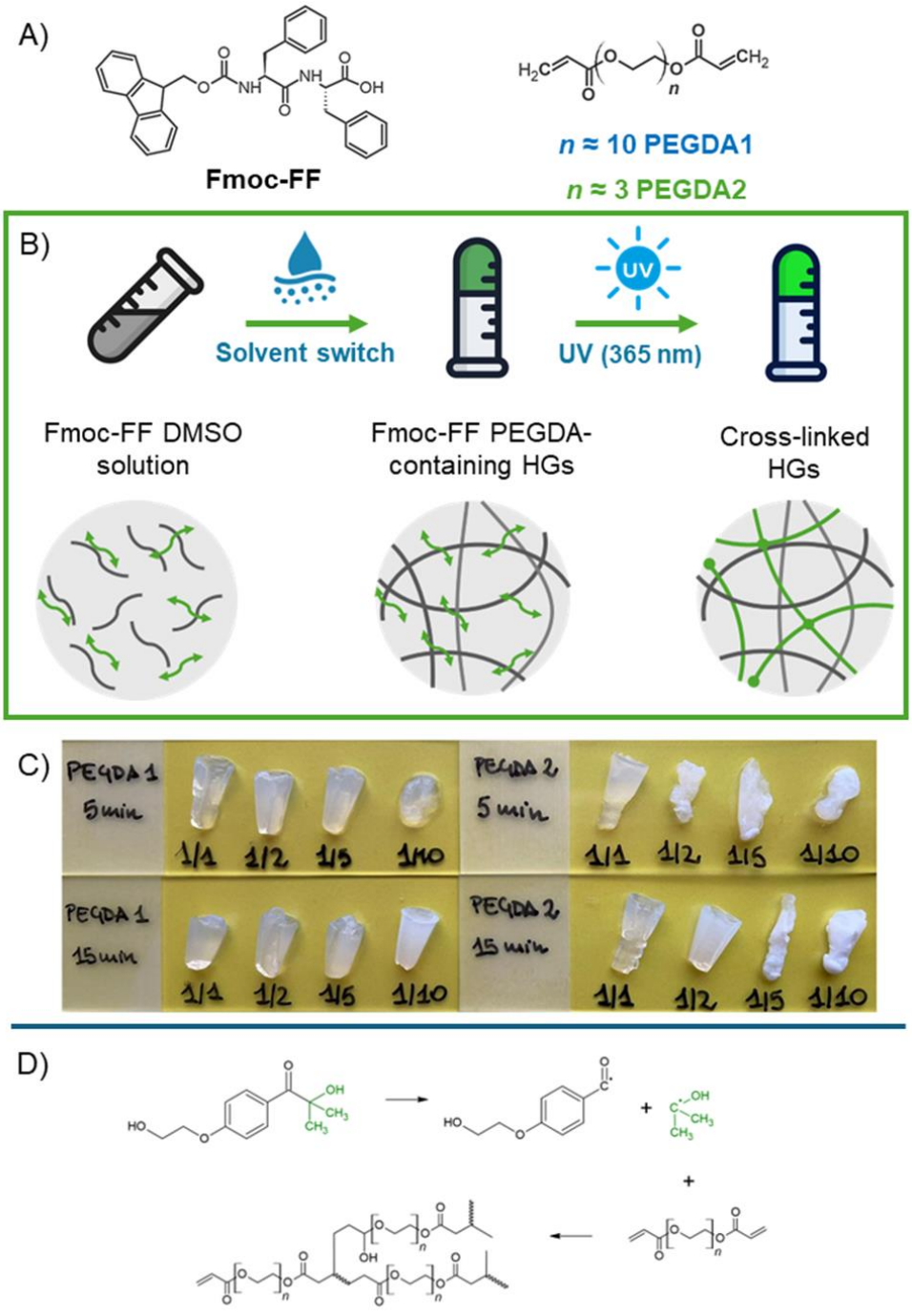

Figure 1: A) Chemical structures of hydrogel components: Fmoc-FF and PEGDA polymers. PEGDA1 and PEGDA2 differ for the average molecular weight (*n*=10 and *n*=3 for PEGDA 1 and PEGDA 2, respectively). **B**) Formulation strategy of mixed hydrogels and their supramolecular schematic representation. **C**) Macroscopical appearance of resulting cross-linked hydrogels after 5 and 15 minutes of UV-Vis irradiation. **D**) Irgacure® 2959 (α-HP) sustained cross-link reaction.

The telechelic nature of the incorporated PEDGA suggests the possibility to generate non-covalent supramolecular\covalent polymeric interpenetrating networks (IPNs) between Fmoc-FF and PEGDA (**Figure 1B and 1C**). Indeed, acrylic groups of polymers can undergo a cross-link reaction under UV-Vis irradiation (365 nm) *via* radical mechanism, in the presence of a photoinducer (**Figure 1D**).[30] In this study, cross-linked HGs were obtained by 2-hydroxy-4′-(2-hydroxyethoxy)-2-methylpropiophenone (or α-HP, Irgacure® 2959) as photoinducer at two different UV-Vis irradiation times (5 and 15 minutes). The cross-linked matrices have been characterized from different points of view to emphasize the emergent properties of the proposed materials, expanding their possible applicative scenario.

Experimental section

Materials and methods:

Fmoc-FF (batch as white lyophilized powder) is commercially available from Bachem (Bubendorf, Switzerland). Poly(ethylene glycol) diacrylate (PEGDA) with an average molecular weight of 575 (PEGDA1) and 250 (PEGDA2) a.m.u., and 2-hydroxy-4′-(2-hydroxyethoxy)-2-methylpropiophenone (namely *α*-HP, Irgacure® 2959) were obtained from Merck (Milan, Italy). All chemicals were used as received unless otherwise stated. UV-Vis measurements were acquired *via* a Thermo Fisher Scientific Inc. (Wilmington, Delaware, USA) Nanodrop 2000c, equipped with a 1.0 cm quartz cuvette (Hellma). UV-Vis measurements were performed using a Perkin-Elmer EnVision 2103-0010 multimode microplate reader.

Formulation of Fmoc-FF/PEGDA/α-HP hydrogel matrices:

Hydrogels were prepared using the DMSO/H_2O "*solvent switch*" strategy as previously reported.[28] Multicomponent matrices (volume of 400 μL, 0.5 wt% Fmoc-FF concentration) were obtained hydrating 20 μL of the Fmoc-FF stock (100 mg/mL) with 380 μL of PEGDA/α-HP solutions. The various Fmoc-FF/PEGDA molar ratios were obtained adding different PEGDA solutions prepared by adding different amounts of pure polymers to α-HP solutions (1.0 mg/mL, 4.46 mmol/L), freshly prepared in double distilled water. The ϕ_{DMSO} (DMSO volume fraction) was kept constant in all the gels at 5%. The metastable and opaque mixtures were vortexed for 3 s and aged at room temperature. The formulative approach was macroscopically evaluated *via* inverted tube test. ρ = 1.11 g/mL and ρ = 1.12 g/mL for PEGDA2 and PEGDA1, respectively.

Cross-link reaction:

Preformed Fmoc-FF/PEGDA/α-HP hydrogel matrices were cross-linked under UV-Vis light exposure at λ=365 nm for 5 or 15 minutes. The irradiation was conducted at a source/sample distance of 2.0 cm using a Vilber UV-handlamp BVL-6.LC (365/254) at a constant 6W (France).

Fourier-transform infrared spectroscopy (FT-IR):

FT-IR analysis (400-4000 cm^{-1} acquisition range) was conducted for the evaluation of the reaction on 250 µL dried samples of each cross-liked gel (0.5 wt%, exposure for 5 min or 15 min) using a Jasco FT/IR 4100 spectrometer (Easton, MD). The exposed samples were dried overnight in CaF_2 cell. Each sample was recorded with a total of 180 scans at a rate of 4 mm/s, sensitivity of 0.40 cm^{-1}, using KBr as background.

*Swelling ratio (*q*) determination:*

Hydrogel swelling ratios (q) were determined as percentage by adding a volume of 1.2 mL of doubly distilled water to each preformed matrix sample (0.50 wt%, V = 400 µL). Samples were incubated overnight at room temperature. The water was then removed, and the sample was weighted to collect the Ws value, representing the weight of the swollen hydrogel. Successively, the sample was freeze-dried and weighed again (Wd). The determined values were used in Equation 1 to calculate the gelling ratio percentage.

$$q = \frac{Ws - Wd}{Ws} \cdot 100 \qquad \text{Eq. (1)}$$

The polymer volume fraction in swollen fashion ($\nu_{2,s}$) was calculated according to Equation 2

$$\nu_{2,s} = \frac{1}{q\left(\frac{\rho}{\rho H2O}\right)+1} \qquad \text{Eq. (2)}$$

M_c (average molecular weight of consecutive crosslinks) values were approximated applying the Peppa-Merrifill equation (Equation 3):

$$\frac{1}{Mc} = \frac{2}{Mn} - \frac{\frac{1}{V}(Log(1-\nu 2,s)+\nu 2,s+\chi(\nu 2,s)^2))}{\rho \nu 2,s\left(\sqrt[3]{(\delta)}-\frac{1}{2}\delta\right)} \qquad \text{Eq. (3)}$$

In which M_n is PEGDA average molecular weight, V is the water molar volume (18 mL mol^{-1}), χ represents the Flory-Huggins polymer-solvent interaction parameter (PEGDA1= 0.40, PEGDA2=0.35), $\nu_{2,r}$ is the polymer fraction in the precursor solution and δ is the ratio $\nu_{2,s}/\ \nu_{2,r}$.

Relaxometry:

NMRD (nuclear magnetic relaxation dispersion) profiles were measured on a SMARtracer fast-field-cycling relaxometer (Stelar S.n.c., Mede (PV), Italy) equipped with a Stelar VTC-91 for temperature

control, from 0.01 to 10 MHz at 25° C. Relaxation rates were measured at 16 different values of the applied magnetic field with an acquisition field of 16.2 MHz, a polarization field of 8.5 MHz, polarization time, and relaxation delay 4 times T1, 16 sampled delay times, and a switching time of 3 ms. Each NMRD profile was fitted according to the same model-free approach used in our previous investigation[28] and reported in equations 6, similarly to that performed on other biomolecules in the presence of two distinct levels of motion (slow and fast).[31,32]

Relaxation rates (R_1) as a function of the proton Larmor frequency ($\upsilon=\gamma B_0/2\pi$) were fitted by using the Equation 4:

$$R_1 = A_0 + \beta\left[\frac{A_1\tau_1}{1+(2\pi\nu\tau_1)} + \frac{A_2\tau_2}{1+(2\pi\nu\tau_2)}\right] \qquad \text{Eq. (4)}$$

Where A_0 is the part of R_1 that remains in the extreme-motional narrowing regime up to the highest sampled frequency, β is the integral of the dispersion profile, τ_1 and τ_2 are the correlation times associated to fast and slow motions, respectively, and A_1 and A_2 are their relative weight coefficients. From parameters of Equation 4, the average correlation time τ_C^{av}, and the percentage of slowly moving water (% slow) can be calculated according to Equations 5 and 6, respectively:

$$\tau_C^{av} = \frac{A_1\tau_1+A_2\tau_2}{A_1+A_2} \qquad \text{Eq. (5)}$$

$$\%\ \text{slow} = \frac{A_2}{A_1+A_2} \qquad \text{Eq. (6)}$$

Rheological analysis:

Rheological analysis on freshly preformed 0.5 wt% hybrid hydrogels (460 µL) was conducted using rotational controlled-stress rheometer (Malvern Kinexus, UK) using a 1.5 cm diameter flat-plate geometry (PU20-PL61). All the measurements were conducted at constant temperature of 25 °C (298 K) in a humidity chamber with a gap distance of 1.0 mm, using preformulated samples. The rheological values, plotted in Pascal (Pa) in logarithmic scale, are reported in terms of storage or elastic modulus (G') and shear loss or viscous modulus (G''), deduced by oscillation strain sweep experiments ($0.1<\omega<100\%$). Frequency sweeps ($0.1<\nu<100$ Hz) were also performed. Tanδ was calculated as G''/G' values.

Morphological and mechanical characterization by Atomic Force Microscopy (AFM):

The morphological and mechanical characterization of the sample surface has been performed at ambient conditions using the AFM NTEGRA (NT-MDT Spectrum Instruments, Moscow, Russia). The high-resolution topographic images have been acquired in semi-contact error mode by means of

NSG01 tips. The NSG01 probes are characterized by a rectangular-shaped cantilever with a pyramidal tip at the apex, having a typical tip curvature radius between 6 and 10 nm. The probes have a resonance frequency comprised between 87 and 230 kHz (typically, 150 kHz) and a mean spring constant of about 5.1 N/m. The AFM topographic images were acquired in Semi-contact error mode over areas of (15×15) μm^2 with a resolution of (768 × 768) points, by setting the setpoint, gain, and rate parameters to about 5.1 nA, 0.9, and 0.4 kHz, respectively. Further topographic acquisitions were taken on areas of (5×5) μm^2 in Semi-contact Phase contrast mode employing NSG01 AFM probes. Those AFM images were acquired at a resolution of (512 x 512) points, setpoint of about 5 nA, gain equal to 1.1, and rate of 0.5 kHz. To suppress the bow and tridimensionality effect, all the AFM topographical acquisition was digitally treated with a second-order plane fit and with a second order flattening filter. The topographic images were analyzed to evaluate the surface roughness. Specifically, it was expressed in terms of root-mean-square surface roughness (R_q), which was quantified by the following equation (Equation 7):

$$R_q = \sqrt[2]{\frac{1}{n}\sum_{1=1}^{n} z_i^2} \qquad \text{Eq. (7)}$$

where n is the number of data points, and zi is the height deviation of the *i-th* point from a mean line, the latter making the arithmetic sum of all zi equal to zero.[33] The roughness analysis was performed over five (5×5) μm^2 areas, randomly chosen on the high-resolution topographic images of both PEGDA1 and PEGDA2 samples. The R_q values were expressed as mean value ± SD.

Software for the analysis of AFM images:

The AFM morphological characterizations were carried out by the NOVA_PX software while the AFM images were analyzed by using the Image Analysis P9 software. Both IA-P9 and NOVA_PX software were obtained from NT-MDT Spectrum Instruments, Moscow, Russia. For each sample, the Fiber orientation analysis was obtained using the OrientationJ tool of the ImageJ 1.47v software (National Institutes of Health, Bethesda, MD, USA). The data were analyzed and plotted by Origin Pro v8 (Origin-Lab Corporation, Northampton, MA, USA).

Small Angle X-ray Scattering (SAXS):

Small Angle X-ray Scattering was performed at B21, Diamond Light Source, UK.[34] Solution samples were loaded into an Arinax liquid handling robot in PCR strips. Samples were then loaded into a quartz capillary. Gel samples were loaded into PEI capillaries loaded into the MPS sample cell.[35] Samples were collected at 20° C, for 21, 1s exposure frames. The sample detector distance was 3.71 m and the wavelength was 0.95 Å. Data was subtracted using ScatterIV.[36]

Captive bubble measurements for contact angle:

The PEGDA1 and 2 samples' surface wettability has been studied by the captive bubble method by using Optical Tensiometer Attention Theta Lite (Biolin Scientific, Finland), equipped with a USB3 Camera (resolution 1280x1024). The samples were fixed on the test plate by means of metallic clamps, and then totally immersed in ultrapure water (MilliQ, surface tension γ = 72.4 mN/m) in a transparent glass cubic container. The air bubbles were manually released against the lower surface of the polymer substrates by using a J-shaped needle with a diameter of about 0.718 mm, which was placed at about 1 mm below the substrate. The angle formed with the surfaces (ϕ) was determined by Young-Laplace equations, injecting a bubble of (5 ± 1) µL in volume beneath samples. The resulting Contact Angle (CA) was calculated by the following Equation 8:

$$CA = 180° - \phi \qquad \text{Eq. (8)}$$

Results and Discussion

Hydrogel formulation and cross-link reaction

Self-supporting multicomponent matrices of Fmoc-FF/PEGDA were generated using the "*solvent-switch*" methodology, by diluting a DMSO peptide stock solution (100 mg/mL) at the final concentration of 0.5 wt% (5.0 mh/mL). The aqueous phase contains both the PEGDA polymer (in different molar ratio, *vide intra*) and the α-HP photoinitiator (Irgacure® 2959, 4.46 mmol/L), allowing the one-step inclusion of both hydrophilic components. The high-water solubility of both PEGDAs was previously exploited for producing multicomponent Fmoc-FF/PEGDA hydrogels at four molar ratios (1/1, 1/2, 1/5 and 1/10 *mol/mol*). [28] It is worth mentioning that the selected PEGDAs molecular weights (MW<1000 Da) should avoid crystalline phases formation, thus promoting a homogeneous PEGDA incorporation in HGs.[29] For all the samples and, as previously observed for Fmoc-FF, the gelation process occurs by an opaque-to-limpid transition, due to the initial formation of peptide clusters able to scatter the light. A gradual macroscopic and homogeneous brightening of the matrices in a few minutes (2-3 minutes), related to the generation of a small-no-scattering entangled fibers networks, follows this step. The absence of syneresis phenomena in the resulting HGs indicates a quantitative entrapment of all the constituents in the hydrogelated matrices. Additionally, no substantial modification of gel kinetics with respect to Fmoc-FF was noted, thus suggesting that both PEGDAs and α-HP cause a negligible interference on the peptide gelation pathway. More specifically, α-HP was selected as type I photoinitiator for its efficient UV light-sensitivity, water solubility, well-established cytocompatibility and high migration of the photolysis fragments due to

its low molecular weight. Additionally, α-HP is a non-yellowing component, stable in solution and with minimal immunogenicity. No substantial macroscopical modification of optical transparency was detected because of Irgacure® 2959 inclusion (data not shown).

The photoinitiator efficient inclusion opened the possibility to induce the cross-link reaction. To evaluate the variable of time exposure, two irradiation times (5 and 15 minutes) were selected. These times were arbitrary chosen and their effect on the macroscopic and the microscopic behavior of the gels was esteemed. After an UV-Vis irradiation (at λ= 365 nm), a α-cleavage reaction occurs, inducing a free-radical photopolymerization involving acrylic moieties of PEGDAs (**Figure 1D**). Due to the evidence that no self-supporting matrices are formed in PEGDAs solutions alone under the same conditions (data not shown), it is believable that the Fmoc-FF dipeptide plays a structural rule in the gelation and cross-link process, allowing the formation of PEGDA containing HGs at concentrations lower than polymers critical gelation ones.

FT-IR analyses

Taking advantage from the substantial modification of the functional groups during the light-induced cross-link reaction, a FT-IR analysis was performed before and after the UV irradiation. FT-IR was conducted on xerogels, in which the pseudo-solid state of the sample allows to reduce the band of water O-H stretching and in turn to facilitate the visualization and interpretation of the bands related to the other functional groups. First, it is important to underline that no substantial IR spectra differences are detectable for all the samples (both PEGDA 1 and PEGDA2 at the different ratios) before the UV exposure (**Figure S1**).

On the contrary, IR imprints changes are observed after the irradiation. Even if discussed for the 1/5 ratio, the following analysis is qualitatively similar to the other Fmoc-FF/PEGDA1 ratios. After 5 minutes of irradiation, an increase of the band at 2920-2880 cm^{-1} (intense C-H aliphatic stretching signal) is detectable for both PEGDA1 and PEGDA2 (see **Figure 2A**). This evidence suggests the formation of C-H bonds, generated by acrylic cross-link reaction. Additionally, the exposition of the hydrogel to irradiation at 365 nm also causes the disappearance of the signal at 1410 cm^{-1} (attributed to deformation of $C=CH_2$) and the substantial decrease in intensity of acylic C=O signal (1193 cm^{-1}, **Figure 2B**). Moreover, a broad band due to the formed primary alcohols is detectable in the 1190-1050 cm^{-1} range (**Figure 2B**). The same modifications are also observed for PEGDA2 containing hydrogels (**Figure S2**).

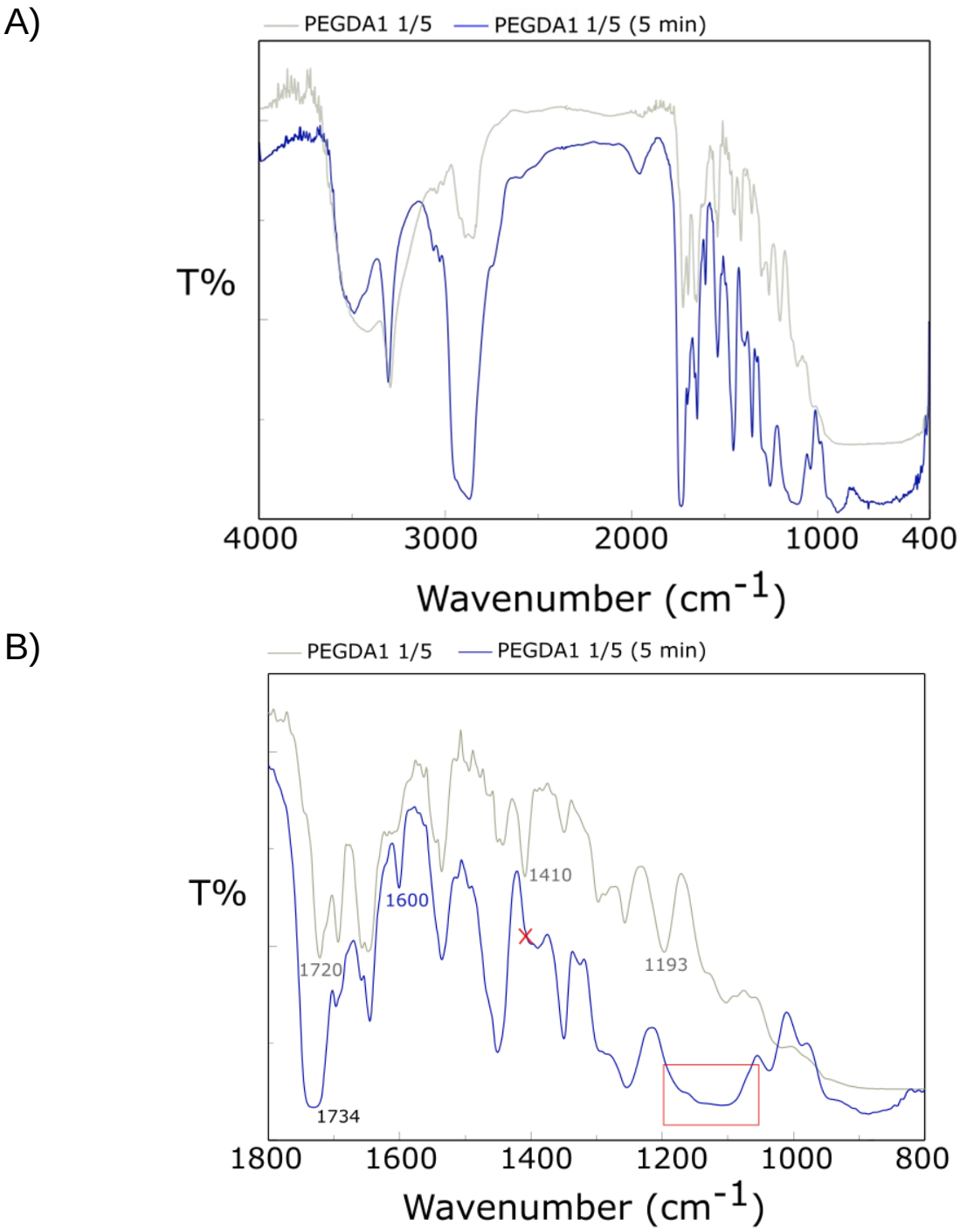

Figure 2: **A**) FT-IR spectra of PEGDA1(1/5) before (grey line) and after 5 minutes (blue line). **B**) Expansion of 1800-800 cm^{-1} range.

Similar IR spectra modifications can be observed for samples irradiated for 15 minutes instead of 5 minutes (**Figure 3A**). However, in this case, the typical C=C stretching signal at 1645 cm^{-1} totally disappears, thus suggesting the complete cross-linking of the PEGDA included in the matrix. Moreover, a progressive shift of the PEGDA carbonyl stretching resonance from 1720 to 1748 cm^{-1} is present, indicating a gradual change in the total chemical environment in carbonyl proximity as

function of the irradiation time (**Figure 3B**). These mutual comparisons between samples further support the hypothesis that the cross-linking reaction is completely achieved after 15 minutes.

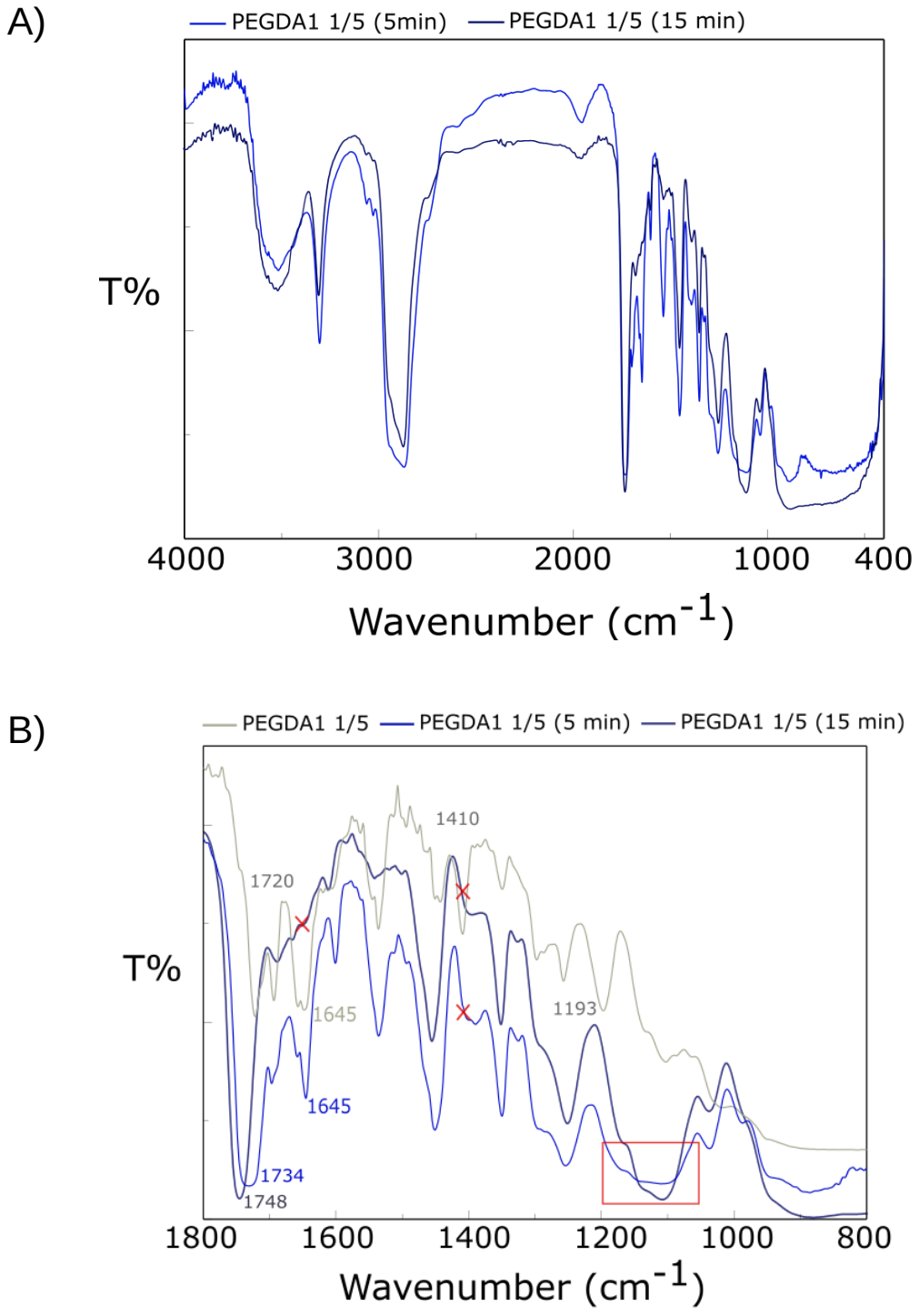

Figure 3: A) FT-IR spectra of PEGDA1 (1/5) 5 minutes (blue line) and 15 minutes (dark blue). **B**) Expansion of 1800-800 cm^{-1} range exposure for 5 minutes (blue line), 15 minutes (dark blue) and starting matrix (grey line).

Macroscopical characterization of gels: optical transparency, water content and water dynamics

Due to the relationship occurring between the macroscopic features of the gels and their final application, both the optical transparency and the water content of the matrices after the UV-Vis irradiation have been evaluated. A macroscopical visualization of matrices, reported in **Figure 1C**, suggests that the irradiation time notably affects the appearance (transparency/opacity) of the gel. The optical transparency was analytically determined *via* UV-Vis spectroscopy at 500 nm (long range), and all the values are collected in **Table 1**. Due to the absence at this wavelength of absorbance peaks attributable to the peptide chromophores, the matrix turbidity can be examined on scattering phenomena. As expected, the transparency of samples decreases with the increasing in time exposure, confirming a linear dependence between the cross-linking degree and the exposure time, with the formation of light scattering supramolecular elements mainly resulting from the density of acrylic mesh. Additionally, the higher opacity associated with matrices containing PEGDA2 (up to 1.603 for 1/10 ratio) suggests a better cross-linking propensity for this polymer, characterized by the lower molecular weight and, therefore, by a lower degree of freedom of the cross-linkable groups.

Table 1: UV-Vis absorbance at 500 nm, swelling ratio (*q*) values, calculated as a percentage according to Equation 1, and number average molecular weight between two consecutive cross-links (M_c).

	PEGDA1				PEGDA2			
	ratio	**Abs (a.u)**	**q (%)**	**M_c g/mol**	**ratio**	**Abs (a.u)**	**q (%)**	**M_c g/mol**
5 min	1/1	0.137	41.5	16.2	1/1	0.169	56.0	14.3
	1/2	0.141	41.3	15.5	1/2	0.275	56.1	14.9
	1/5	0.209	39.5	14.1	1/5	0.700	55.4	14.1
	1/10	0.221	41.3	12.8	1/10	0.741	55.5	12.3
15 min	1/1	0.137	41.2	16.3	1/1	0.164	54.7	15.4
	1/2	0.155	39.0	15.8	1/2	0.290	56.0	13.7
	1/5	0.230	38.2	14.3	1/5	0.961	56.2	12.7
	1/10	0.283	37.8	12.1	1/10	1.603	59.1	11.2

Further information on the supramolecular organization and on the permeation properties of the gel were obtained by studying the water behavior by swelling ratio evaluation and by measuring the longitudinal relaxation rate (R1 = 1/T1) as a function of the applied magnetic field. The swelling ratio (*q*) was determined as percentage by calculating the difference between the gel weight before and after overnight incubation in water. From the inspection of the *q* values, collected in **Table 1**, no significant differences can be detected between samples at different molar ratios, thus suggesting that the relative polymer amount into the hybrid matrix does not affect the water entrapment. On the other

hand, an increase of *q* (up to 55%) is observed for PEGDA2-containing hydrogels, independently from the irradiation time. Moreover, all the samples have a *q* value significantly higher if compared to those previously found for the corresponding not cross-linked hydrogelated matrices and to the nude Fmoc-FF HGs (*q* = 29.7%). The higher cross-linked *q* values seem counterintuitive. Indeed, a lower swelling capacity could be expected because of an increasing of the irradiation time. This result may connect the chemistry and the features of the materials, indicating a major polymer volume fraction in swollen state for PEGDA2 samples. This evidence is indicative of a better cross-link for PEGDA2-containing HGs that, in virtue of its shorter PEG moiety, should be more accessible to establish hydrogen bonds in the hydrogel.[37] Consequently, a rough estimation of cross-link density was achieved by applying the Peppas-Merrill model.[38] The relationship between the matrices cross-linking, the UV exposure and the polymer ratios was also inspected calculating the number average molecular weight between two consecutive polymer bonds (M_c). M_c values (**Table 1**), in the range of 16.3-11.2 g/mol, decreases as the UV irradiation time increased, thus signifying the formation of dense highly cross-linked networks with multiple entanglement. As expected, the network density increases with the increasing of PEGDA amount, and PEGDA2-containing matrices resulted in a denser hydrogel.

The study of water dynamics within the hydrogel structure has been explored through a relaxometric method. The examination of changes in the Relaxation rate (R_1) across various water-containing substances in response to varying magnetic fields (NMRD-Nuclear Magnetic Resonance Dispersion profiles) has commonly been employed to quantify dynamic parameters linked to two distinct levels of water movement: a slower one, attributed to water molecules confined within the hydrogel framework, and a faster one, associated with more freely moving water molecules.[39,40]

^{1}H-NMRD profiles of cross-linked Fmoc-FF/PEGDA1 and Fmoc-FF/PEGDA2 hydrogels at two molar ratios (1/1 and 1/10 *mol/mol*) and irradiated for 5 or 15 minutes are reported in **Figure 4A** and **4B**. Data were fitted according to the model-free approach described by Equation 6 and fitting parameters are collected in **Table 2**. The analysis was performed for these two couples of samples, assuming them as are more representative ones.

Both the percentage of slow motion (% slow) and the average correlation time (τ_C^{av}) of all the samples are notably higher compared to those previously observed for the respective not crosslinked hydrogel matrices and similar to those found for the Fmoc-FF HG alone.[28] By the inspection of graphs of **Figure 4C** and **Figure 4D**, it can be concluded that no significant changes in the average correlation time occur by changing the PEG length (PEGDA1 *vs* PEGDA2), the relative amount of the two components into the hybrid matrix (1/1 *vs* 1/10) or the irradiation time (5 min *vs* 15 min). On the

contrary, some trends are observed by looking at the integral of the dispersion profiles (β), which can be associated to the amount of entrapped water, and the percentage of slowly moving water (% slow).

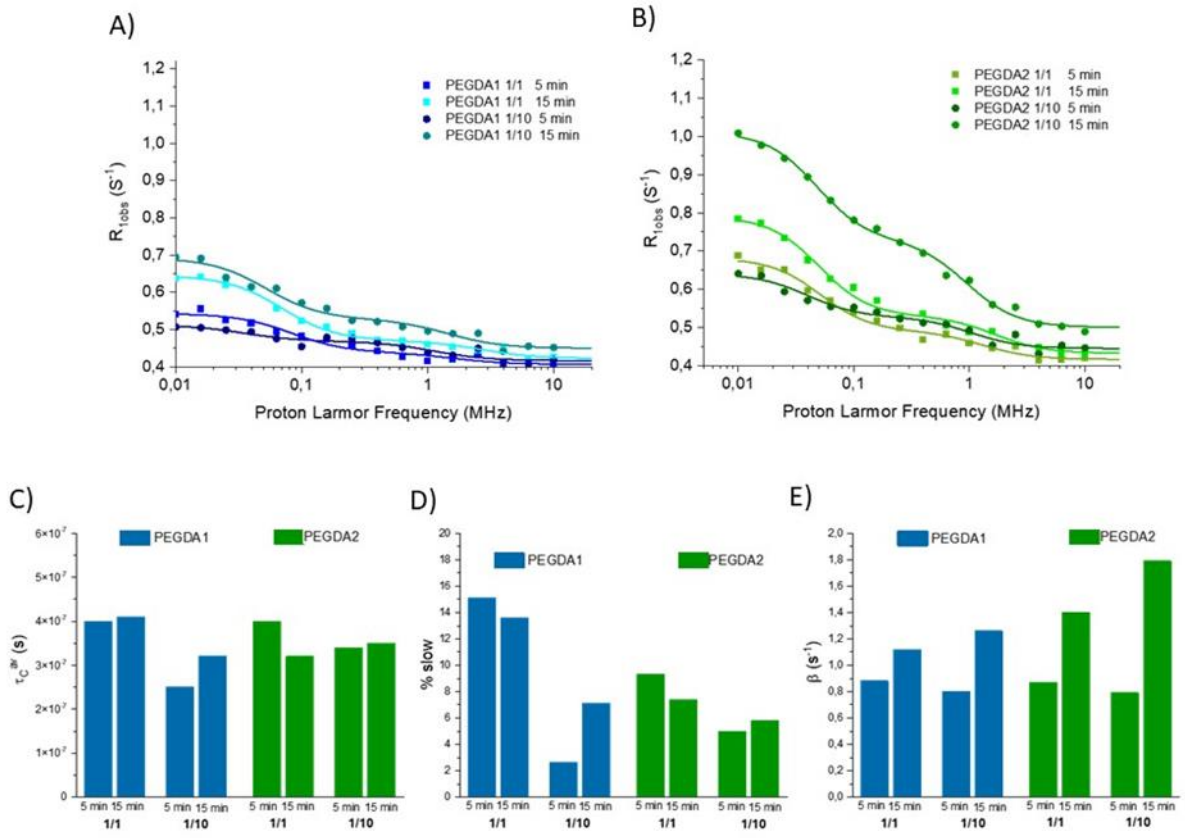

Figure 4: ^{1}H NMRD profiles measured at 298K on HGs with cross-linked PEGDA1 (**A**) and PEGDA2 (**B**) for 5 and 15 minutes and different molar ratios (1/1 and 1/10 *mol/mol*). Continuous lines represent the best fits obtained with a sum of Lorentzian functions. Variation of **C**) the average water correlation time (τ_c^{av}), **D**) the percentage of slow-moving water (% slow) and **E**) the integral of NMRD dispersion profiles (β) calculated from fitting of ^{1}H NMRD profiles reported in panel A and B as a function of PEGDA1 and PEGDA2 molar ratios (1/1 or 1/10) and irradiation times (5 or 15 min).

In particular, β values are higher for hydrogels irradiated for longer times, by increasing the amount of polymers within the matrix and containing PEGDA2 with respect to PEGDA1. This latter result is perfectly consistent with the data concerning the swelling ratio, supporting the occurrence of a higher water entrapment capacity for PEGDA2-containing hydrogels, despite being characterized by shorter PEG chain. On the other hand, the amount of water exhibiting a slower kinetics motion (% slow) appears to be inversely proportional to the polymer quantity within the matrix (1/1 > 1/10) and directly proportional to the length of the PEGDA chain (PEGDA1 > PEGDA2). Overall, these observations lead to the conclusion that hydrogels based on the use of PEGDA2 exhibit a greater

capacity to incorporate water into the matrix compared to those containing PEGDA1, and that the freedom of movement of these water molecules increases with the hydration extent.

Table 2: Best-fit parameters of the 1H-NMRD profiles of the hybrid hydrogels.

	System	A_0 (s^{-1})	β (s^{-1})	A_1	τ_1 (s)	A_2	τ_2 (s)	% slow*	τ_C^{av} (s)
PEGDA1	(1/1) 5 min	0.40	0.98	3.2×10^5	1.0×10^{-7}	5.5×10^4	4.3×10^{-6}	14.7	3.7×10^{-7}
	(1/1) 15 min	0.43	1.17	6.8×10^5	5.9×10^{-8}	6.5×10^4	2.4×10^{-6}	8.7	2.5×10^{-7}
	(1/10) 5 min	0.42	0.70	5.2×10^5	1.4×10^{-7}	1.4×10^4	3.0×10^{-6}	2.6	2.5×10^{-7}
	(1/10) 15 min	0.45	1.26	5.6×10^5	1.1×10^{-7}	4.3×10^4	3.2×10^{-6}	7.1	3.2×10^{-7}
PEGDA2	(1/1) 5 min	0.42	1.33	4.6×10^5	1.2×10^{-7}	4.6×10^4	3.1×10^{-6}	9.2	4.0×10^{-7}
	(1/1) 15 min	0.43	1.2	8.6×10^5	9.5×10^{-8}	6.8×10^4	3.2×10^{-6}	7.3	3.2×10^{-7}
	(1/10) 5 min	0.45	0.77	6.4×10^5	1.8×10^{-7}	2.6×10^4	6.2×10^{-6}	3.9	4.2×10^{-7}
	(1/10) 15 min	0.52	1.5	6.0×10^5	2.5×10^{-7}	4.9×10^4	3.7×10^{-6}	7.5	5.1×10^{-7}

Rheological analysis

The rheological analysis allows evaluating the mechanical properties of the cross-linked matrices prepared by UV-Vis irradiation. For this, using a plate geometry, the loss (G') and the storage (G'') moduli were extrapolated in the regime of viscoelastic region (at 0.1 % strain) by the strain sweep experiment (460 µL, 0.01-100 % strain range, 1.0 Hz, **Figure S3-S4**) for each sample. The G' and G'' values are plotted in **Figure 5A** and **5B** for PEGDA1 and PEGDA2 HGs, respectively, and collected in **Table 3.** For all the samples the G' value is higher than the corresponding G'' one (G'>G''), thus analytically confirming the no-Newtonian flow behaviour, associated with the existence of a gel state. The rheological analysis previously performed on not cross-linked HGs highlighted that the inclusion of the PEGDA polymers into the Fmoc-FF hydrogel causes an increase of the stiffness of the matrix at all the investigated molar ratios.[28] It is reasonable to suppose that the G' increase in cross-linked HGs because of the establishment of further intermolecular interactions occurring between the PEGDA polymer, water and the Fmoc-FF dipeptide fibres.

Independently by the irradiation time, the rise of UV irradiation produces more rigid materials with respect to untreated systems. For all the PEGDA1 containing HGs a progressive and quasi-linear G' value decrease is detected with the increase of the polymer fraction (Figure 5A). The general loss of rigidity in samples with the increase of PEGDA1 amount may be attributed to the uncompleted (5 minutes) or more flexible (15 minutes) diacrylates networks, reducing the ability of peptide fibres and polymer to interact cooperatively at the supramolecular level.

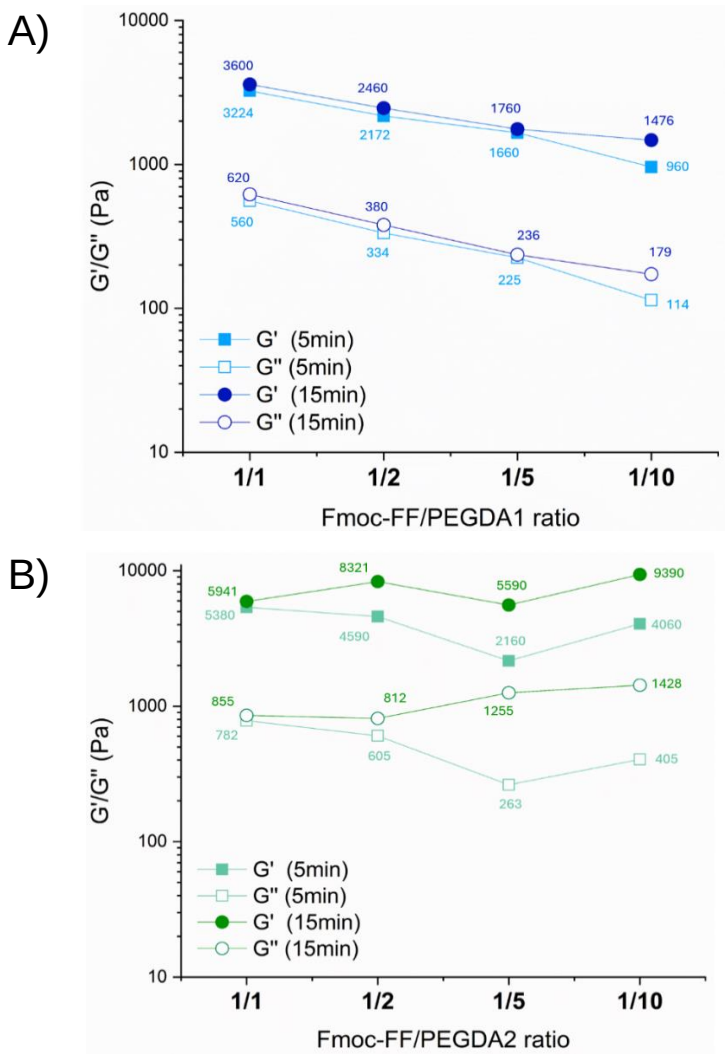

Figure 5: Diagram reporting the storage (G') and the loss (G'') moduli of cross-linked hydrogels (5 and 15 minutes) as function of the molar ratio for PEGDA1 (**A**) or PEGDA2 (**B**) containing matrices.

On the contrary, cross-linked PEGDA2 HGs exhibit comparable/major G' values with respect to untreated systems, without a general trend related to peptide/polymer ratios noticed for PEGDA1 series (**Figure 5B**). However, also in this case, an increase in the UV time exposure produced more rigid materials.

The mutual analysis of rheological data is indicative of a better reticulation for PEGDA2 multicomponent matrices, with a direct correlation between G' values and crosslinking density (V_c), as supported by the theory of rubber elasticity, ($G' = V_cRT$).[41] The polymer amount, as the exposure time was found able to increase both the breakage point of strain (ω_c) and of frequency (from 25 Hz to 50 Hz, **Figure S5-S6**). Specifically, PEGDA2 systems (15 min) are associated to a monotone increase of both mechanical moduli with frequency (**Figure S6**). This trend, independent from the peptide/PEGDA2 ratio, is indicative of an increase in the elastic response because of the decreasing

dissipative stress time. Finally, the tanδ loss factor (tanδ =ratio G''/G', **Table 3**), can give additional information about the material's viscoelastic behaviour, reporting that lower values of tanδ are associated to more pronounced elastic properties. Tanδ values progressively decrease with the increase of peptide/polymer ratios for PEGDA1 series and for PEGDA2 at 5 min.

Overall, the rheological analysis on mixed systems indicated the possibility of controlling the viscoelastic properties of the matrices as function of both components features and irradiation times, generating a plethora of matrices with different chemistry and response in terms of mechanical properties and rheological behaviour.

Table 3: Hydrogel rheological analysis. Extrapolated storage modulus (G') and loss modulus (G") from oscillation strain sweeps are reported, as tanδ (G''/G'), breakage point of strain (ω_c) and frequency (ν_c).

		5min					***15 min***				
	Ratio	**G'(Pa)**	**G''(Pa)**	**tanδ**	**ω_C (%)**	**ν_c (Hz)**	**G'(Pa)**	**G''(Pa)**	**tanδ**	**ω_C (%)**	**ν_c (Hz)**
PEGDA1	1/1	3224	560	0.173	16	32	3600	620	0.172	20	35
	1/2	2172	334	0.154	17	35	2460	380	0.154	28	35
	1/5	1660	225	0.135	9	39	1760	236	0.134	11	43
	1/10	960	114	0.118	26	49	1476	179	0.121	30	60
PEGDA2	1/1	5380	782	0.145	16	-	5941	855	0.144	27	-
	1/2	4590	605	0.132	18	-	8321	812	0.117	31	-
	1/5	2160	263	0.122	14	-	5590	1255	0.224	43	-
	1/10	4060	45	0.100	38	-	9390	1428	0.152	54	-

Atomic Force Microscopy (AFM)

The high-resolution AFM images of both PEGDA1 and PEGDA2 multicomponent hydrogels at 1/1 and 1/10 *mol/mol* ratios were acquired in Semi-contact error mode. This couple of samples were selected as the two extremes of both series to empathize expected differences. Using the reported operation mode, the cantilever oscillation amplitude varies based on the sample's surface topography. The feedback loop aims to maintain a specified cantilever oscillation amplitude (Set Point) by adjusting the reference Magnitude signal (Mag), which is proportional to the oscillation amplitude. However, due to the feedback loop's inertia, it cannot instantly compensate for variations in the magnitude signal. More in detail, the Mag signal reflects the current cantilever oscillation amplitude and serves as the error signal for the feedback loop, providing additional information on surface topography. By observing the AFM images in **Figure 6A** and **6B**, the surface of FmocFF/PEGDA1 samples, exposed to both 5 and 15 minutes of UV treatment, appears almost flat and no relevant nano- or microstructures are present on the surfaces (**Figure S7**). However, the hydrogel surfaces exposed

for a longer time to UV light appear slightly more homogeneous and flatter than the samples exposed for a shorter time (**Figure 6B**).

On the other hand, the surfaces of the PEGDA2 containing HGs are irregular and inhomogeneous for both the exposure times (**Figure 6C and 6D**). Moreover, in the PEGDA2 samples, fibrillar-like networks are visible on the sample surfaces. This phenomenon is more evident for the PEGDA2 containing HGs characterized by elevated polymer ratios (1/5 and 1/10 *mol/mol*), exposed to UV light for 15 minutes (**Figure S8**).

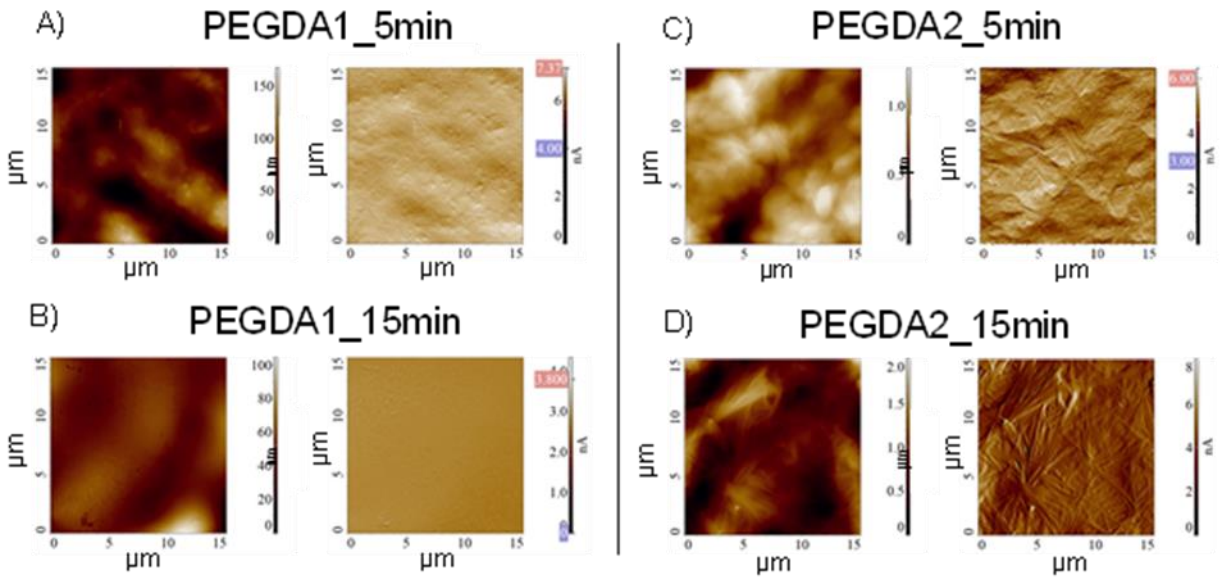

Figure 6: Representative high-resolution AFM characterization, acquired in Semi-contact error mode on (15x15) μm^2 areas, of PEGDA1 1/10 *mol/mol* **A**) and **B**) PEGDA2 1/10 mol/mol **C**) and **D**), exposed at UV-Vis irradiation for 5 and 15 minutes, respectively. For each AFM characterization, the Height image is shown on the left side while the Magnitude image is reported on the right.

The Rq measurements further confirmed these experimental findings. As reported in **Figure 7**, the surface roughness of PEGDA1 containing hydrogels, polymerized for 5 minutes, decreased from 42.98 ±6.34 nm to 9.40 ± 1.38 nm for the 1/1 and 1/10 *mol/mol*, respectively. A similar trend was observed for samples exposed for 15 minutes whose *Rq* values vary from 61.92 ± 6.94 nm to 8.70 ± 1.53 nm. On the other hand, PEGDA2 HGs polymerized for 5 minutes exhibit a higher roughness respect to PEGDA1 ones, but a slight decrease can be observed between the surface of the samples at different molar ratios (181.10 ± 3.19 nm and 160.14 ± 3.19 nm for 1/1 and 1/10, respectively). Similarly, also their counterparts polymerized for 15 minutes, that are less rough, show a slight decrease for 1/1 and 1/10 *mol/mol* HGs (68.48 ± 3.53 nm and 58.96 ± 5.07 nm, respectively). The noticeable disparities between the PEGDA1 and PEGDA2 reinforce a sort of correlation between

polymer molecular weight and the matrices' topological features, likely attributed to variations in the network of chemical bonds. This physicochemical parameter further influenced the interaction networking between peptides and polymers, resulting in distinct surface morphologies within the hybrid matrices.

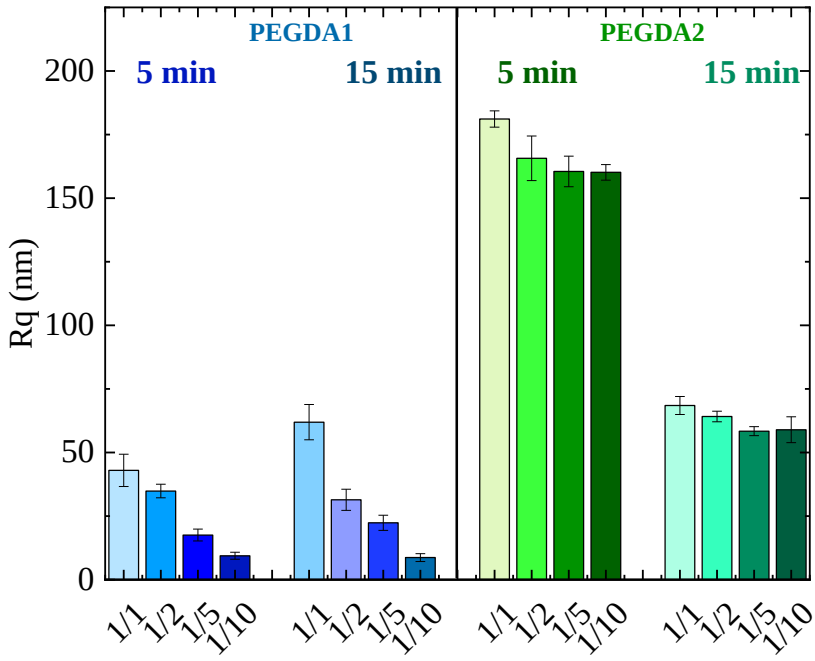

Figure 7: R_q mean values calculated by averaging the roughness of 5 different (5x5) μm^2 areas, randomly selected on the topographic AFM images of the PEGDA1 and 2 samples. The error bar represents the standard deviation.

To further investigate the supramolecular organization of the fibrillar network, AFM images were acquired at higher magnification in Semi-contact Phase Contrast mode. The phase signal, along with the amplitude of the cantilever oscillation, highlights edges and, consequently, produces images with higher contrast compared to the topography images. Indeed, the phase is strongly influenced by several physical-chemical characteristics of the sample surface, such as the hardness, elasticity, and adhesion between the AFM probe and the sample surface. Through the Phase Contrast imaging mode, it is possible to better appreciate the qualitative differentiation between various materials at the surface by comparing features that are exclusively visible in the phase images and not in the topography ones.[41] The assessment of specific mechanical properties from phase differences is generally unattainable due to phase dependence on a plethora of diverse physical properties. Several studies assert that regions characterized by darker phases (i.e., smaller, or more negative phase values) correspond to softer materials,[43,44] whereas alternative studies propose the converse relationship.[45,46] By observing the AFM topography images of the PEGDA1 samples on the Height channel, the

presence of fibers mesh close to the surface can be glimpsed at higher magnification (**Figure S9**). Indeed, the small height differences measured on the surface do not allow us to clearly distinguish the fibers network while it is clearly visible on the AFM Phase images, due to the strong contrast (**Figure 8A, and 8C**).

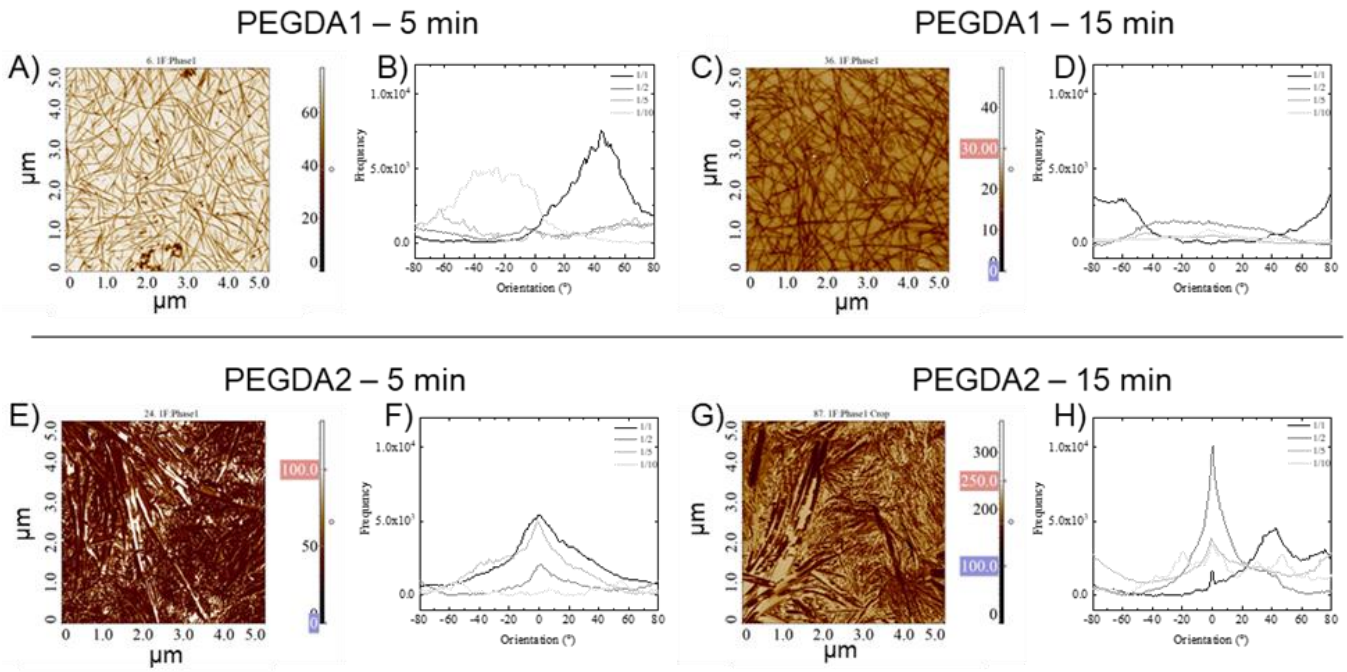

Figure 8: Representative AFM Phase-contrast images acquired (5 x 5) µm^2 areas of PEGDA1 containing HGs exposed to UV-Vis light for **A**) 5 and **C**) 15 minutes, respectively. AFM Phase-contrast images of PEGDA2 contianing matrices samples, after **E**) 5 and **G**) 15 minutes of UV-Vis light exposure. The graphs depict the fibers orientation distributions of **B**) and **D**) PEGDA1 matrices for UV-Vis light for 5 and 15 minutes, respectively and **F**) and **H**) PEGDA2 HGs exposed to UV-Vis light for 5 and 15 minutes, obtained from the OrientationJ plugin in ImageJ software.

The fibers are characterized by a darker phase (here, in a range of 60°), and they seem to be randomly organized in the network. Moreover, the amount of fibers decreases with the increase of the Fmoc-FF/PEGDA1ratio, independently from the UV exposure time (**Figure S9**). A similar trend was found in the PEGDA2 samples (**Figure S10**). However, in all the PEGDA2 samples, an increase in the fiber number, as well as in the fibers dimension was observed, as shown in the **Figure 8E** and **7G**. The AFM phase images were further analyzed with the OrientationJ tool in ImageJ software to measure the alignment of the fibers network. The orientation of the fibers in Fmoc-FF/PEGDA1 (1/1 *mol/mol*) samples exposed to UV light for 5 minutes shows a high peak around 45 degrees while no relevant peaks were observed in the other PEGDA1 samples (**Figure 8B** and **BD**). On the other hand, in the

PEGDA2/Fmoc-FF, both polymerized at 5 and 15 minutes, robust peaks at around 0 degrees were observed. Furthermore, the height of the orientation peaks decreases with the increase of the PEGDA2/Fmoc-FF ratio (**Figure 8F and 8H).**

Small Angle X-ray Scattering (SAXS)

SAXS measurements were performed to obtain detailed information on the fibril structure (i.e. dimensions and internal density). The SAXS data for all samples are shown in **Figure 9**. It was possible to fit the higher wavenumber *q* part of the data to a model form factor for long core-shell cylinders, consistent with the fibrillar morphology observed by AFM.

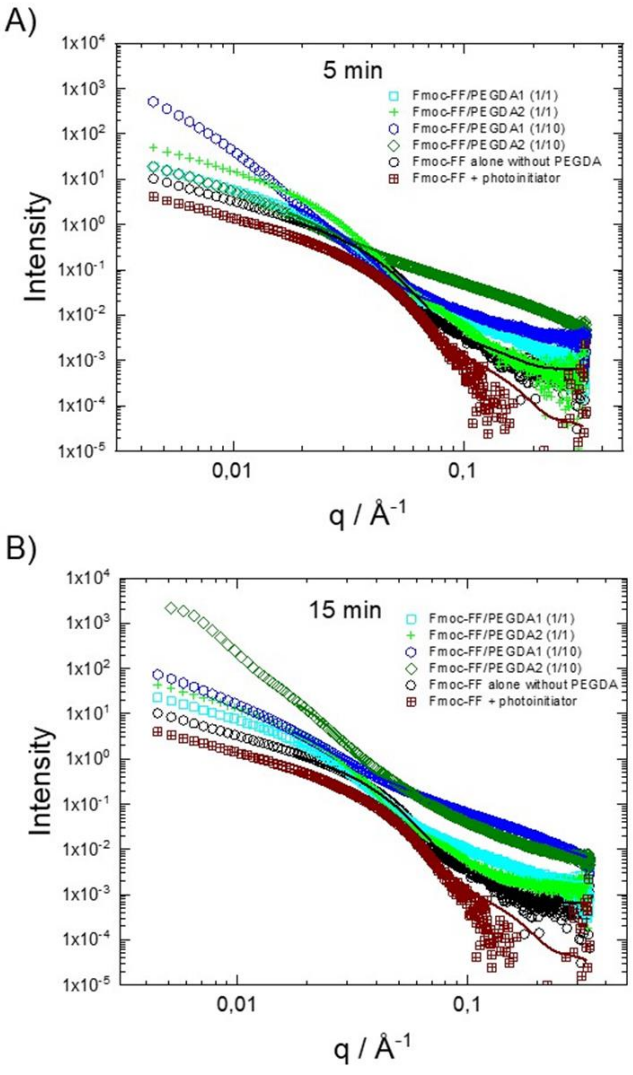

Figure 9: SAXS data for samples cross-linked for 5 (**A**) and 15 minutes (**B**). Every fifth data point plotted for ease of visualization. The lines (with same colour scheme as data points) represent the model form factor fit described in the text (form factor fit parameters in Table S1).

A contribution of a power law background is included to allow for unaggregated Fmoc-FF/polymer chains (with intensity slope approximately = 2). The low *q* part of the data is influenced by structure factor effects and was not included in the form factor fitting.[47] The corresponding fit parameters are listed in Table S1. These show a core radius R = 38.0 - 47.4 Å with significant polydispersity around 20 Å for all samples, with little significant variation from sample to sample for the cross-linked samples. The core radius is significantly lower for the two Fmoc-FF samples without PEGDA. The core radius corresponds approximately to the expected length of the Fmoc-FF conjugate with some inclusion of PEGDA cross-linker for the corresponding samples. The shell thickness is ΔR = 39.5 – 70.9 Å for all samples and is generally larger for the PEGDA cross-linked samples. This is expected since the shell should incorporate the ends of PEGDA chains (the remainder of which presumably occupy the interstitial space in the hydrogels). The shell thickness is similar for all samples. The values of cylinder length L listed in Table S1 do not show significant variation, considering that $L >> R$, this just contributes to scaling of the intensity which varies from sample to sample. A notable trend from the fit parameters in Table S1 is that the shell scattering contrast η_{shell} increases for the PEGDA (1/10 *mol/mol*) samples compared to the PEGDA (1/1 *mol/mol*) samples. Also performing pairwise comparisons, the core scattering contrast η_{core} is reduced (with one exception). This definite trend points to a significant reduction in core/shell scattering contrast for the PEGDA (1/10 *mol/mol*) samples compared to PEGDA (1/1 *mol/mol*) which reflects the increased amount of PEGDA in the shell for the former case, which also leads to a reduction in core scattering density.

Contact Angle

The wettability of the sample surface, characterized by the captive bubble method (**Figure S11**), was quantified in terms of contact angle, and the results are reported in **Figure 10**. All the samples exhibited a markable hydrophilic behaviour (θ >90), however the hydrophilicity decreased with the increase of the Fmoc-FF/PEGDA1 and PEGDA2 molar ratio. With respect to PEGDA1/Fmoc-FF (1/1) the contact angle value increased to 33 % in PEGDA1/Fmoc-FF (1/10) sample polymerized for 5 minutes, whereas this percentage become equal to 78% in the sample polymerized for 15 minutes. A similar trend was observed from the analysis Fmoc-FF/PEGDA2 (1/10) respect to their counterpart (1/1): specifically, when samples were polymerized at 5 min the contact angle augmented up to 22% with respect to its counterpart (1/1), while, a more marked increase of the contact angle was found in the Fmoc-FF/PEGDA2 samples, exposed at UV irradiation for 15 minutes, increasing up to about 75% in the Fmoc-FF/PEGDA2 (1/10).

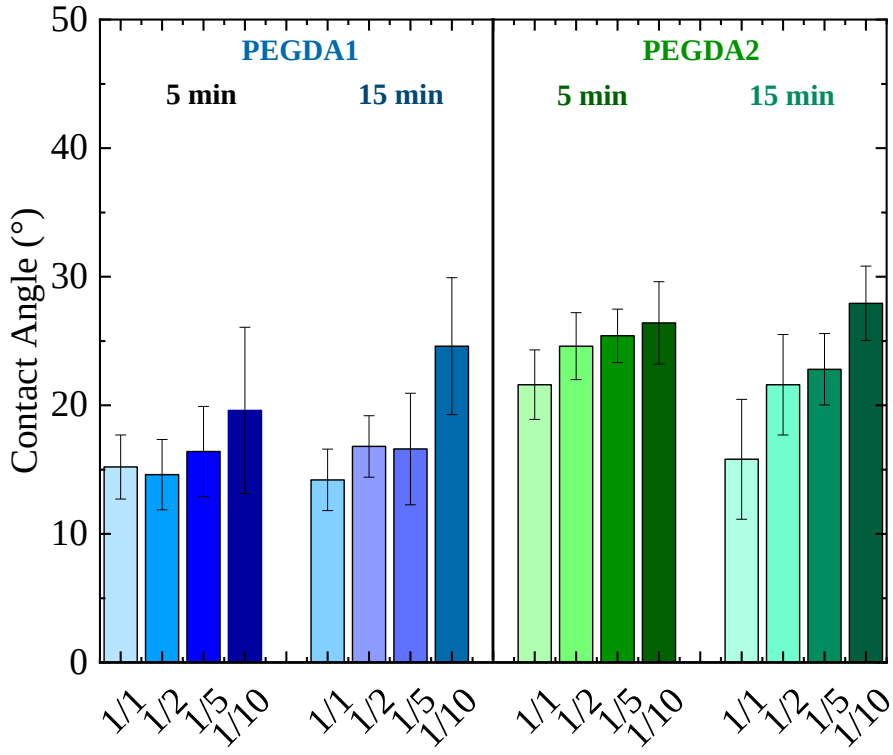

Figure 10: PEGDA/Fmocc-FF contact angles measured by the captive bubble method. The graph shows the estimated contact angle mean value, acquired on five areas of the Fmoc-FF/PEGDA1 and PEGDA2 samples, exposed to UV-Vis irradiation for 5 and 15 minutes. The error bar represents the standard deviation.

Conclusions

The in-depth characterization of the proposed systems allowed establishing that several factors (*e.g.* polymerization time, polymer molecular weight, peptide/PEGDA ratio) are variable able to clearly influence the material properties, connecting the chemistry of building blocks to their final emerging features. The rule of Fmoc-FF as structuration peptide adjuvant is evident, too. The inclusion of Fmoc-FF permits the generation of PEGDA-based networks at low polymer concentration. Additionally, the explored variables are easily manageable, suggesting an efficient scalability of the proposed materials to application routes. The evaluated parameters influence the hydrogel rigidity, transparency, and topography as well as the water packing and mobility. Additionally, the multicomponent systems can serve as nanostructured and supramolecular tools in different macroscopical fashion, as bulk material or films. The capability to engineer the physicochemical characteristics the Fmoc-FF/PEGDA hydrogels, xerogels and films paves the way for their application in numerous fields. The formulative route, well-matched with shapeability requirements, is compatible the spin-coating approach. The multicomponent matrices can be suitable as soft substrates for AFM-based nanolithography,[48] enlarging the substrates for flow-chemistry, lab on chip

or biosensing and electro-optical systems.[49,50] The viscoelasticity is indicative of developments of stretchable support for smart wearable devices,[51] and flexible components for organic plastic electronics.[52] In each of these instances, scientific research thrives with fervour, driven by the imminent technological revolution and the imperative of energy transition. This endeavour is directed towards developing progressively superior wearable devices, crafted from environmentally sustainable and renewable materials.

Acknowledgments

We thank Diamond Light Source for the award of beamtime SM26698-18.

Supporting information description

The Supporting Information is available free of charge. **S1**. FT-IR spectra of Fmoc-FF multicomponent hydrogels containing PEGDA1 (1/1 mol/mol) or PEGDA2 (1/10 mol/mol) before cross-linking reaction. **S2.** Comparison of FT-IR spectra of 1/5 PEGDA1 and PEGDA2 after cross-linking of 5 minutes. **S3.** Strain sweeps for 5 minutes and 15 minutes crosslinked PEGDA1 containing systems. **S4**. Strain sweeps for 5 minutes and 15 minutes crosslinked PEGDA2 containing systems. **S5.** Frequency sweeps for 5 minutes and 15 minutes crosslinked PEGDA1 containing systems. **S6.** Frequency sweeps for 5 minutes and 15 minutes crosslinked PEGDA1 containing systems. **S7.** High-resolution AFM topographic images, acquired in Semi-contact error mode on (15 x 15) μm^2 areas, of Fmoc-FF/PEGDA1 systems (5 and 15 minutes) at different polymer molar ratios (1/1, 1/2/, 1/5/, and 1/10 mol/mol). **S8.** High-resolution AFM topographic images, acquired in Semi-contact error mode on (15 x 15) μm^2 areas, of Fmoc-FF/PEGDA2 systems (5 and 15 minutes) at different polymer molar ratios (1/1, 1/2/, 1/5/, and 1/10 mol/mol). **S9:** AFM topographic images, acquired in Semi-contact Phase Contrast on (5 x 5) μm^2 areas at a resolution of (512 x 512) points, Fmoc-FF/PEGDA1 sample, treated under UV-Vis irradiation for 5 and 15 minutes at different polymer molar ratios (1/1, 1/2/, 1/5/, and 1/10 *mol/mol*). **S10:** AFM topographic images, acquired in Semi-contact Phase Contrast on (5 x 5) μm^2 areas at a resolution of (512 x 512) points, Fmoc-FF/PEGDA2 sample, treated under UV-Vis irradiation for 5 and 15 minutes at different polymer molar ratios (1/1, 1/2/, 1/5/, and 1/10 *mol/mol*). **S11.** Contact angle measurements, performed in the captive bubble configuration, of PEGDA1 and PEGDA2 containing matrices at different polymer molar ration (1/1, 1/2/, 1/5/, and 1/10 *mol/mol*) and exposed at UV-Vis irradiation for 5 and 15 minutes.

References

(1) Alberstein, R.; Suzuki, Y.; Paesani, F.; Tezcan, F.A. Engineering the entropy-driven free-energy landscape of a dynamic nanoporous protein assembly. *Nat. Chem.* **2018**, *10*, 732–739.

(2) Sun, H.; Li, Y.; Yu, S.; Liu, J. Hierarchical self-assembly of proteins through rationally designed supramolecular interfaces. *Front. Bioeng. Biotechnol.* **2020**, *8*, 295

(3) Buehler, M.J. Nature designs tough collagen: explaining the nanostructure of collagen fibrils. *PNAS* **2006**, *103*, 12285–12290.

(4) Solomonov, A.; Shimanovich, U. Self-assembly in protein-based bionanomaterials. *Isr. J. Chem.* **2020**, *60(12)*, 1152–1170.

(5) Levin, A.; Hakala, T. A.; Schnaider, L.; Bernardes, G. J. L.; Gazit, E.; Knowles, T. P. J. Biomimetic peptide self-assembly for functional materials. *Nature Rev. Chem.* **2020**, *4*, 615–634.

(6) Huo, Y.; Hu, J.; Yin, Y.; Liu, P.; Cai, K.; Ji, W. Self-assembling peptide-based functional biomaterials. *Chem. Eur. J.* 2023, 24(2), e202200582.

(7) Whitesides, G.M.; Boncheva M. Beyond molecules: self-assembly of mesoscopic and macroscopic components. *Proc. Natl. Acad. Sci. U S A.* **2002**, *99(8)*, 4769–4774.

(8) Pochan, D.; Scherman, O. Introduction: molecular self-Assembly. *Chem. Rev.* **2021**, *121(22)*, 13699–13700.

(9) Reches, M.; Gazit, E. Self-assembly of peptide nanotubes and amyloid-like structures by charged-termini-capped diphenylalanine peptide analogues. *Isr. J. Chem.* **2005**, *45*, 363–371.

(10) Zozulia, O.; Marshall, L.R.; Kim, I.; Kohn, E.M.; Korendovych, I.V. Self-assembling catalytic peptide nanomaterials capable of highly efficient peroxidase activity. *Chem. Eur. J.* **2021**, *27(17)*, 5388–5392.

(11) Brightwell, D.F.; Truccolo, G.; Samanta, K.; Fenn, E.J.; Holder, S.J.; Shepherd, H.J.; Hawes, C.S.; Palma, A. A reversibly porous supramolecular peptide framework. *Chem. Eur. J.* **2022**, *28(66)*, e202202368.

(12) Gazit, E. Reductionist approach in peptide-based nanotechnology. *Annu. Rev. Biochem.* **2018**, *20(87)*, 533–553.

(13) Bertolani, A.; Pizzi, A.; Pirrie, L.; Gazzera, L.; Morra, G.; Meli, M.; Colombo, G.; Genoni, A.; Cavallo, G.; Terraneo, G.; Metrangolo P. Crystal structure of the DFNKF segment of human calcitonin unveils aromatic interactions between phenylalanines. *Chem. Eur. J.* **2017**, *23*, 2051–2058.

(14) Dasgupta, A.; Mondal, J. H.; Das, D. Peptide hydrogels. *RSC Adv.* **2013**, *3*, 9117–9149.

(15) Diaferia, C.; Rosa, E.; Gallo, E.; Smaldone, G.; Stornaiuolo, M.; Morelli, G.; Accardo, A. Self-Supporting Hydrogels Based on Fmoc-derivatized cationic hexapeptides for potential biomedical applications. *Biomedicines* **2021**, *9(6)*, 678.

(16) Mitrovic, J.; Richey, G.; Kim, S.; Guler, M. O. Peptide hydrogels and nanostructures controlling biological machinery. *Langmuir* **2023**, *39(34)*, 11935–11945.

(17) Jayawarna, V.; Ali, M.; Jowitt, T. A.; Miller, A. F.; Saiani, A.; Gough, E.; Ulijn, R. V. Nanostructured hydrogels for three-dimensional cell culture through self-assembly of fluorenylmethoxycarbonyl–dipeptides. *Adv. Mater.* **2006**, *18(5)*, 611–614.

(18) Mahler, A.; Reches, M.; Rechter, M.; Cohen, S.; Gazit, E. Rigid, self-assembled hydrogel composed of a modified aromatic dipeptide. *Adv. Mater.* **2006**, *18(11)*, 1365–1370.

(19) Smith, A. M.; Williams, R.J.; Tang, C.; Coppo, P.; Collins, R.F.; Turner, M.L.; Saiani, A.; Ulijn. R.V. Fmoc-diphenylalanine self assembles to a hydrogel via a novel architecture based on π–π interlocked β-sheets. *Adv. Mater.* **2008**, *20(1)*, 37–41.

(20) Diaferia, C.; Rosa, E.; Morelli, G.; Accardo, A. Fmoc-diphenylalanine hydrogels: optimization of preparation methods and structural insights. *Pharmaceuticals* **2022**, *15(9)*, 1048.

(21) Mayans, E.; Aleman, C. Revisiting the self-assembly of highly aromatic phenylalanine homopeptides. *Molecules* **2020**, *25(24)*, 6037.

(22) Orbach, R.; Adler-Abramovich, L.; Zigerson, S.; Mironi-Harpaz, I.; Seliktar, D.; Gazit, E. Self-assembled Fmoc-peptides as a platform for the formation of nanostructures and hydrogels. *Biomacromol*. **2009**, *10(9)*, 2646–2651.

(23) Dudukovic, N.A.; Zukoski. C.F. Mechanical properties of self-assembled Fmoc-diphenylalanine molecular gels. *Langmuir* **2014**, *30(15)*, 4493–4500.

(24) Levine, M.S.; Ghosh, M.; Hesser, M.; Hennessy, N.; Di Guiseppi, D.M.; Adler-Abramovich, L.; Schweitzer-Stenner, R. Formation of peptide-based oligomers in dimethylsulfoxide: identifying the precursor of fibril formation. *Soft Matter* **2020**, *16*, 7860–7868.

(25) Raeburn, J.; Mendoza-Cuenca, C.; Cattoz, B.N.; Little, M.A.; Terry, A.E.; Cardoso, A.Z.; Griffiths, P.C.; Adams, D. J. The effect of solvent choice on the gelation and final hydrogel properties of Fmoc–diphenylalanine. *Soft Matter*, **2015**, *11*, 927–935.

(26) Diaferia, C.; Rosa, E.; Gallo, E.; Morelli, G.; Accardo, A. Differently N-capped analogues of Fmoc-FF. *Chem. Eur. J.* **2023**, *29(28)*, e202300661.

(27) Diaferia, C.; Morelli, G.; Accardo, A. Fmoc-diphenylalanine as a suitable building block for the preparation of hybrid materials and their potential applications. *J. Mater. Chem. B* **2019**, *7*, 5142–5155.

(28) Rosa, E.; Gallo, E.; Sibillano, T.; Giannini, C.; Rizzuti, S.; Gianolio, E.; Scognamiglio, P. L.; Morelli, G.; Accardo, A.; Diaferia. C. Incorporation of PEG diacrylates (PEGDA) generates hybrid Fmoc-FF hydrogel matrices. *Gels* **2022**, *8(12)*, 831.

(29) Liu, J.; Hou, X.; Park, H. B.; Lin, H. High-performance polymers for membrane CO_2/N_2 separation. *Chem. Eur. J.* **2016**, *22(45)*, 15980–15990.

(30) Choi, J. R.; Yong, K. W.; Choi, J. Y.; Cowie, A. C. Recent advances in photo-crosslinkable hydrogels for biomedical applications. *BioTechniques* **2019**, *66(1)*, 40–53.

(31) Halle, B.; Jóhannesson, H.; Venu, K. Model-free analysis of stretched relaxation dispersions. *J. Magn. Reson.* **1998**, *135*(1), 1-13.

(32) Bertini, I.; Fragai, M.; Luchinat, C.; Parigi, G. 1H NMRD profiles of diamagnetic proteins: a model-free analysis. *Magn. Reson. Chem.* **2000**, *38*, 543–550.

(33) Gadelmawla, E.S.; Koura, M.M.; Maksoud, T.M.A.; Elewa, I.M.; Soliman, H.H. Roughness parameters. *J. Mater. Process. Technol.* **2002**, *123*, 133–145.

(34) Cowieson, N. P. Edwards-Gayle, C. J. C.; Inoue, K.; Khunti, N.S.; Doutch,J.; Williams, E.; Daniels, S.; Preece, G.; Krumpa, N.A.; Sutter, J.P.; Tully, M.D.; Terrill N.J.; Rambo, R.P. Beamline B21: high-throughput small-angle X-ray scattering at Diamond Light Source. *J. Synchrotron Radiat.* **2020**, *27*, 1438–1446.

(35) Edwards-Gayle, C. J. C.; Khunti, N.; Hamley, I.W.; Inoue, K.; Cowieson, N.; Rambo, R. Design of a multipurpose sample cell holder for the Diamond Light Source high-throughput SAXS beamline B21. *J. Synchrotron Radiat.* **2021**, *28*, 318–321.

(36) Rambo, R. (2009). BIOISIS, http://www.bioisis.net/

(37) Cavallo, A.; Madaghiele, M.; Masullo, U.; Lionetto, M.G.; Sannino, A. Photo-crosslinked poly(ethylene glycol) diacrylate (PEGDA) hydrogels from low molecular weight prepolymer: Swelling and permeation studies. *J. App. Pol. Sci.* **2017**, *134(2)*, app.44380.

(38) Cruise, G.M. Scharp, D. S.; Hubbell, J.A. Characterization of permeability and network structure of interfacially photopolymerized poly(ethylene glycol) diacrylate hydrogels. *Biomaterials* **1998**, *19(14)*, 1287–1294.

(39) Mikac, U.; Sepe, A.; Gradišek, A.; Kristl, J.; Apih, T. Dynamics of water and xanthan chains in hydrogels studied by NMR relaxometry and their influence on drug release. *Int. J. Pharm.* **2019**, *563*, 373–383.

(40) Ravera, E.; Fragai, M.; Parigi, G.; Luchinat, C. Differences in dynamics between crosslinked and non-crosslinked hyaluronates measured by using fast field-cycling relaxometry. *ChemPhysChem* **2015**, *16*, 2803–2809.

(41) Raman, T.S.; Kuehnert, M.; Daikos, O.; Scherzer, T.; Krömmelbein, C.; Mayr, S.G.; Abel, B.; Schulze, A. A study on the material properties of novel PEGDA/gelatin hybrid hydrogels polymerized by electron beam irradiation. *Front. Chem.* **2023**, *10*, 1094981.

(42) Raghavan, D.; Gu, X.; Nguyen, T.; VanLandingham, M.; Karim, A: Mapping polymer heterogeneity using atomic force microscopy phase imaging and nanoscale indentatio. *Macromolecules* **2000**, *33*, 2573–2583.

(43) Haviland, D.B.; van Eysden, C.A.; Forchheimer, D.; Platz, D.; Kassab, H.G.; Leclère, P. Probing viscoelastic response of soft material surfaces at the nanoscale. *Soft Matter*, **2016**, *12*, 619 *Soft Matter*, **2016**, *12*, 619–624.

(44) Sauer, B.B. McLean, R.S.; Thomas, R.R. Tapping Mode AFM Studies of nano-phases on fluorine-containing polyester coatings and octadecyltrichlorosilane monolayers. *Langmuir* **1998**, *14*, 3045–3051.

(45) McLean, R.S.; Sauer, B.B. Tapping-mode AFM studies using phase detection for resolution of nanophases in segmented polyurethanes and other block copolymers, *Macromolecules* **1997**, *30*, 83148317.

(46) Werner, E.; Güth, U.; Brockhagen, B.; Döpke, C.; Ehrmann, A. Examination of polymer blends by AFM phase images. *Technologies* **2023**, *11*, 56.

(47) Hamley, I. W., Small-Angle Scattering: Theory, Instrumentation, data and applications. Wiley: Chichester, **2021**.

(48) Vincenti, L.; Pellegrino, P.; Farella, I.; Cascione, M.; De Matteis, V.; Quaranta, F.; Rinaldi, R. Fabrication of 3D nanostructures via AFM-based nanolithography. *Proceedings* **2024**, *97*, 56.

(49) Su, Z.; Yang, Y.; Huang, Q.; Chen, R.; Ge, W.; Fang, Z.; Huang, F.; Wang, X. Designed biomass materials for “green” electronics: a review of materials, fabrications, devices, and perspectives. *Prog. Mat. Sci.* **2022**, *125*, 100917.

(50) Hui, Z.; Zhang, L.; Ren, G.; Sun, G.; Yu, H-D.; Huang, W. Green flexible electronics: natural materials, fabrication,and applications. *Adv. Mater.* **2023**, *35*, 2211202.

(51) Gao, L.; Zhu, C.; Li, L.; Zhang, C.; Liu, J.; Yu,H-D.; Huang, W. All paper-based flexible and wearable piezoresistive pressure sensor. *ACS Appl. Mater. Interf.* **2019**,*11*, 25034–25042.

(52) Pilotto Cenci, M. Eco-friendly electronics: a comprehensive review. *Adv. Mater. Technol.* **2022**, *7*, 2001263.

Table of content

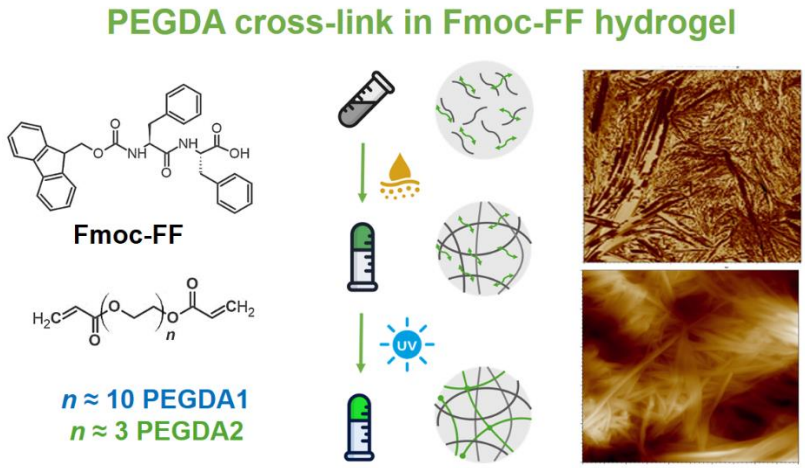

Fmoc-FF hydrogels support the cross-link of PEGDAs polymers, generating multivalent materials as function of peptide/polymer ratio and UV-Vis exposure time.